Methods[1]

Expedition 331 Scientists[2]

Chapter contents

Introduction

This chapter documents the methods used for shipboard scientific analyses, including sample collection, preparation, and preservation for either shipboard or shore-based analysis. This information can be used to understand how we arrived at preliminary conclusions and interpretations and to provide information for those interested in ancillary analyses, shore-based sampling, or integrative investigations.

This chapter also covers coring techniques, core handling, and the numbering of sites, holes, cores, sections, and samples. In most cases, this information mirrors the details described in previous volumes of the *Proceedings of the Integrated Ocean Drilling Program*. However, the information will differ from previous drilling expeditions undertaken with the D/V *Chikyu*, as Integrated Ocean Drilling Program (IODP) Expedition 331 is not part of the Nankai Trough Seismogenic Zone Experiment (NanTroSEIZE) program.

Site locations

Expedition 331 site locations were selected based on preexpedition surveys, including tagging of potential sites using the deep submergence vehicles (DSVs) *Shinkai* 2000 and 6500. Final sites were selected after remotely operated vehicle (ROV) seafloor surveys during the expedition.

Onboard Global Positioning System (GPS) satellite navigation was used to position the vessel using dynamic positioning, and acoustic beacons deployed on the seafloor provided additional means of acquiring and keeping vessel position during operations. When the ROV was deployed, a precise fix on the location of the borehole was obtained upon spud-in.

Drilling operations

Four coring systems were employed during Expedition 331:

1. A hydraulic piston coring system (HPCS) equivalent to the advanced piston corer (APC) employed on the R/V *JOIDES Resolution*,
2. An extended shoe coring system (ESCS) equivalent to the extended core barrel (XCB) employed on the *JOIDES Resolution*,
3. An extended punch coring system (EPCS), and
4. A Baker Hughes INTEQ (BHI) 4 inch diameter industrial coring system.

[1]Expedition 331 Scientists, 2011. Methods. *In* Takai, K., Mottl, M.J., Nielsen, S.H., and the Expedition 331 Scientists, *Proc. IODP,* 331: Tokyo (Integrated Ocean Drilling Program Management International, Inc.). doi:10.2204/iodp.proc.331.102.2011
[2]**Expedition 331 Scientists' addresses.**

doi:10.2204/iodp.proc.331.102.2011

Drilled intervals are initially referred to in meters drilling depth below seafloor (DSF), which is measured from the kelly bushing on the rig floor to the bottom of the drill pipe and later converted to core depth in meters below seafloor (mbsf). When sediments of substantial thickness cover the seafloor, the mbsf depth of the seafloor is determined using a mudline core combined with the length of the drill string at the time of shooting the first core.

The mudline core is taken by tagging the seafloor with the drill bit, lifting the bit to a point <9.5 m off bottom, and shooting a partial HPCS core. Water depth is either estimated from pressure using a sensor on the ROV or calculated by subtracting the distance from the rig floor to sea level from the mudline measurement (DSF). Depths of core tops (mbsf) are determined by subtracting seafloor depth (DSF) from core top depth (DSF). The resulting core top data (mbsf) are the ultimate reference for any further depth calculation.

Drilling-induced core deformation

X-ray computed tomography (CT) imagery and direct inspection of split cores often reveal significant evidence for disturbance of recovered materials. HPCS-related disturbance includes the concave downward appearance of originally horizontal bedding and liquefaction features related to differential compaction of layers with different competency and pore fluid content, as well as the suction-induced flow of significant amounts of exotic material into the bottom of incomplete HPCS penetrations. ESCS/BHI-related disturbance includes rotation and "spiraling" of sections of cores, "biscuiting" of small sections of core and injection of either drilling mud or finely ground material produced at the drill bit into spaces between individual biscuits, or brecciation or grinding of material before collection into the core liner/core barrel. Core deformation may also result from depressurization, expansion, and thermal equilibration of the core as it travels up the drill string, during handling on deck, and during core cutting and splitting. Where possible, such core disturbance was noted in core descriptions.

Numbering of sites, holes, cores, sections, and samples

Sites drilled by the *Chikyu* are numbered consecutively from the first site with a prefix "C" because the site is drilled using the Center for Deep Earth Exploration (CDEX) platform. A site usually refers to one or more holes drilled while the ship is positioned within 300 m of the first hole. However, because of the closeness of several of the Expedition 331 sites, site here also refers to a group of holes with the same set of objectives, a set that differs from those of other groups of holes that may be within 300 m. The first hole drilled at a given site is assigned the site number modified by the suffix "A," the second hole takes the site number and the suffix "B," and so forth. These suffixes are assigned regardless of recovery, as long as penetration takes place.

During Expedition 331, we drilled at Sites C0013 (proposed Site INH-4D), C0014 (proposed Site INH-5D), C0015 (proposed Site INH-11A), C0016 (proposed Sites INH-1C and INH-1D), and C0017 (proposed Site INH-6B).

During Expedition 331, the *Chikyu* occupied Holes C0013A–C0013H, C0014A–C0014G, C0015A–C0015C, C0016A and C0016B, and C0017A–C0017D.

Cored intervals are calculated based on an initial 9.5 m length, which is the standard core barrel length for each coring system. Partial penetration of the HPCS core barrel is generally detectable during coring by measurement of the pressure drop in the hydraulic system that powers the piston core. Partial pressure drop and gradual release of pressure are used to calculate the estimated penetration depth in these cases. In addition, we specified the collection of 4.5 m long coring intervals (half-cores) in areas of extreme interest thought to contain fragile or fractured rocks in fault zones. Expansion of cores in the upper sections (and sucked-in material) and gaps related to unrecovered material result in recovery percentages greater or less than 100%, respectively.

Depth intervals are assigned starting from the depth below seafloor at which coring started (mbsf). Because this was the only method used, all depths below seafloor are referred to as mbsf.

Short cores (incomplete recovery) are all assumed to start from that initial depth by convention.

A core recovered with the HCPS/ESCS/EPCS systems is typically divided into 1.5 m long sections that are numbered serially from 1 beginning at the top. When the BHI system was used, section length was set at 75 cm.

For all systems, material recovered from the core catcher was assigned to a separate section, labeled core catcher (CC), and placed at the bottom of the lowermost section of the recovered core.

A full identification number for a sample consists of the following information: expedition, site, hole, core number, core type, section number, and top to bottom interval in centimeters measured from the top of the section. For example, a sample identification of "331-C0013D-2H-5, 80–82 cm," represents a sample removed from the interval between 80 and

82 cm below the top of Section 5 of the second HPCS core from Hole C0013D during Expedition 331 (Fig. F1). All IODP core identifiers indicate core type. The following abbreviations are used:

H = HPCS.
X = ESCS.
T = EPCS.
L = BHI.

Core handling

The following section describes in detail the core flow from the drill floor through the laboratory to storage (Fig. F2). Four different coring systems were deployed during Expedition 331, which required two different core cutting areas and different retrieval procedures, as well as different procedures for sectioning of cores and handling of fast-tracked samples. The use of aluminum liners for HPCS/EPCS/ESCS coring also lead to adjustment of core handling.

HPCS/ESCS/EPCS core handling

The standard methods of coring used during Expedition 331 were changed little or not at all from previous procedures. As soon as a core was retrieved on deck, the core catcher was delivered to the core cutting area. A sample was taken for paleontological analysis, and the remainder of the core catcher sample was packed into the core liner and curated. The whole core was then delivered to the core cutting area.

At the core cutting area, the recovered core length and the total length of void space were measured, and core identification, length, drilling advance, and depth information were entered into the J-CORES database. If cores contained gas in void spaces, void gas samples were collected at this time through a hole drilled into the liner. Collection was not possible when ship-standard coring systems were used with aluminum liners.

The core was divided into sequentially numbered sections, and the sections were cut. Pairs of small (5 cm^3) plugs of sediment were removed from the bottom of appropriate core sections for headspace gas analysis. All sections were then taken to the core processing deck and scanned by X-ray CT for choosing whole-round samples for microbiology and interstitial water squeezing. Oversight by a sedimentologist or geochemist acting as a "watchdog" was required before the interstitial water whole round was squeezed. If the watchdog rejected a sample, a new interstitial water sample was chosen. Each section was then sealed at the top (blue cap) and bottom (white cap); yellow caps indicate removed whole-round core samples (with the sample code marked on the end cap). All sections were marked and labeled, data were entered into the J-CORES database, and sections were moved to the core processing deck.

BHI 4 inch core

BHI cores were brought up in barrels of 9–27 m lengths at a time. If cores longer than 9 m were taken, they consisted of two to three 9 m aluminum inner tubes and were cut into 9 m sections that were processed one at a time. These cores were processed at a separate core cutting area behind the derrick of the *Chikyu*. Because the cores were laid down behind the derrick and handled by BHI core techs, a team consisting of the Curator and a science party member trained for H_2S conditions assisted in this core cutting area in labeling the liner, taking headspace gas samples, and evaluating the potential for whole-round sampling based on the exposed cross sections of the otherwise opaque aluminum core liners.

Sections of BHI core are nominally 0.75 m long, which made them manageable for a single person and which fit in the onboard storage racks at two per rack. Cores were between 9 and 18 m in length. Each section was cut by pushing the core under a waxed diamond-blade rotary saw, starting from the top. Based on the quality of the cross section, sections were scored for whole-round potential and set aside in a cage. When all sections were cut, the highest ranked sections were carried to the regular core cutting area, bagged if measured H_2S exceeded safe levels, and taken into the laboratory.

Shipboard general measurement plan

Core flows for 2.44 and 4 inch core sections were similar from the time the sections entered the laboratory, except that some multisensor core logger for whole-round samples (MSCL-W; Geotek Ltd., London, UK) measurements could not be run on the 4 inch cores because of size and on the aluminum-lined 2.44 inch cores because of liner material.

Core catcher material was sampled for paleontology studies. At Site C0013 no fossils were found, so core catcher samples were used to support and elaborate on findings by the visual core description (VCD) group using scanning electron microscopy.

Because the sampling plan called for frequent paired whole-round samples for microbiology and pore water geochemistry, all sections were brought to the X-ray CT and scanned. Based on these images, whole-round samples were cut and sent either to squeezing in the sample preparation room or to the microbiology laboratory for further sampling.

The remaining sections were scanned using the MSCL-W for magnetic susceptibility, *P*-wave velocity (PWV), noncontact resistivity, gamma ray attenuation (GRA) density, and natural gamma radiation (NGR). For the 4 inch cores, only GRA and NGR could be run. Scans were completed after equilibration to room temperature of 20°–22°C, which usually meant allowing the cores to cool.

Next, unsplit cores were subjected to thermal conductivity measurements, followed by splitting into archive and working halves. The working halves were further sampled for X-ray diffraction (XRD) and moisture and density (MAD) measurements.

Archive halves went to the MSCL imaging system (MSCL-I) and then to the VCD group of petrologists and sedimentologists. After core description, archive halves were taken to the MSCL 3-D gantry (MSCL-XYZ) and scanned spectrophotometrically.

Both archive and working halves were then wrapped in double layers of cling film, bagged, sealed, and stored at 4°C in the core reefer.

H_2S precautions

Many cores released H_2S gas in concentrations >200 ppmv (detection limit) when sectioned. Rather than let them vent, these were often taken straight to the laboratory after being wrapped in airtight bags. These sections were scanned in the bags on the X-ray CT scanner and cut for whole-round sampling in a fume hood if necessary. These cores were then allowed to vent in the draft chamber before further processing.

The areas where H_2S was released were the whole-round cutting area and the core splitting room. When split, the freshly exposed longitudinal sections at times gave off enough gas to require self-contained breathing apparatus (SCBA) packs to be worn during splitting. Split sections were then allowed to sit in the draft room to degas.

Downhole logging

Two advanced piston corer temperature tool (APCT3) probes were available for Expedition 331. These were calibrated for the range 0°–55°C and were not designed to survive for long at much higher temperatures. We used these probes only for the uppermost two cores at Site C0014 and the uppermost seven cores at the cooler Site C0017. At higher temperatures we used commercial thermoseal (Nichiyu Giken Co., Ltd.) strips taped to the outer surface of the core liner. These adhesive strips have embedded, chemically impregnated wafers that turn black when exposed to the designated temperature. Each strip contained five wafers calibrated in 5° or 10°C increments and covered one of several limited ranges between 75° and 210°C.

Lithostratigraphy

X-ray computed tomography

X-ray CT imaging provides information about lithological features without the need for core splitting. Images were used to assist in deciding locations for obtaining whole-round samples and also to provide a guide to core loggers of which lithologies had been removed by whole-round sampling. We followed the methodology documented in the "cookbook" (X-ray CT Scanner, version 3.00, 31 July 2007) prepared by CDEX/Japan Agency for Marine Earth Science and Technology (JAMSTEC), as well as methods used during previous expeditions (e.g., IODP Expedition 319). The X-ray CT instrument on the *Chikyu* is a GE Yokogawa Medical Systems LightSpeed Ultra 16 capable of generating sixteen 0.625 mm thick slice images every 0.5 s, the time for one revolution of the X-ray source around the sample. The protocol is based on GE Healthcare (2006), Mees et al. (2003), and Nakano et al. (2000). Data generated for each core consist of core-axis-normal planes of X-ray attenuation values with dimensions of 512 × 512 pixels. These data were stored as Digital Imaging and Communication in Medicine (DICOM) formatted files.

Visual core descriptions

We described working halves of cores on a section-by-section basis to document lithological information together with descriptions of hydrothermal alteration and mineralization (Mazzullo and Graham, 1988). Lithological features were observed visually and recorded in section-scale templates using the shipboard database software J-CORES. Along with alteration and sulfide mineralization (see **"Petrology"**), lithological descriptions were then included on the section-scale VCDs using Strater software. The Lithology column on each VCD plots all beds that are ≥2 cm thick to scale. Interlayers <2 cm thick are identified as laminae in the Structures/Veins column.

The classification scheme for clastic lithology follows Mazzullo et al. (1988). Texture (defined by the relative proportions of sand, silt, and clay) follows the classification of Shepard (1954). We did not use separate patterns for more heavily indurated examples of the same lithologies (e.g., silty clay versus silty claystone) because the distinction is somewhat arbitrary.

Graphic patterns for all lithologies encountered during Expedition 331 are summarized in Figure **F3.** Also shown are symbols for sedimentary structures,

soft-sediment deformation structures, severity of core disturbance, and features. Note that sulfide-rich sediments were coded as "massive sulfide sediment," "sulfidic sand," or "sulfidic mud" in the Lithology column and further described using petrographic nomenclature described in **"Petrology."**

Particle size analysis

Particle size analysis can improve the characterization of fine-grained biogenic sediments. Particle size variations can also be used to evaluate lithological/textural controls and effects of microbial activity on biogenic sediments. Grain size analysis is a classic sedimentological tool commonly used for the study of siliciclastic deposits, where particle sizes reflect the processes that generated the clasts, including weathering, erosion, transport, and sedimentation. Despite the dominant application for siliciclastic sediments, grain size studies of fine-grained biogenic sediments have been widely performed (Paull et al., 1988; McCave et al., 1995; Stuut et al., 2002).

We used the multiwavelength laser particle analyzer (LS; Beckman Coulter, model LS13320) to measure the grain size of core sediments. Laser particle analysis is based on the principle that particles of a given size diffract light through a given angle, which increases with decreasing particle size. A parallel beam of monochromatic light is passed through a suspension, and the diffraction light is focused onto a multielement ring detector. The detector senses angular distribution of scattered light intensity (Syvitski, 1991; McCave et al., 1995). The laser particle analyzer can provide rapid, automated, and precise measurement of sediment grain size ranging from 0.375 µm to 2 mm in size in ~10 min, including a rinse stage. The LS used is equipped with a micro volume module (MVM) system, and the autosampler allows the user to load a run of 30 samples to be processed automatically. The accompanying software calculates the grain size distribution of the sample and appropriate statistics. Data may be exported to external programs.

When measuring the particle size distribution of siliclastic sediments, care must be taken to inhibit the formation of aggregates from true sedimentary particles (Ramaswamy and Rao, 2006) unless the analysis of aggregates formed from biogenic/authigenic components is intended. In the case of sediments, the formation of aggregates is most notable within the finer (smaller grain size) fractions when free organic phases or iron oxide precipitates tightly bind sedimentary particles into aggregates (Syvitski, 1991). Furthermore, organic particles and aggregates may have shapes, geometries, and other surface properties that interfere with routine laser particle size analysis of siliclastic sediments. During this expedition, an aliquot of a 0.5 g subsample was used for measuring grain size. When necessary, organic matter was removed by oxidizing with 10% v/v H_2O_2, whereas interference from other nonsiliclastic biogenic/authigenic components, including carbonates and phosphates, was reduced by acidifying samples with 10% v/v HCl at room temperature.

Grain size distributions are displayed as phi (Φ) values, which is a base two logarithmic scale commonly utilized to represent grain size information for a sediment distribution. Logarithmic phi values (in base two) are calculated from particle diameter size measures in millimeters as follows:

$$\Phi = -\log_2 d = -(\log_{10} d/\log_{10} 2),$$

where d = particle size in millimeters.

A comparison of grain sizes in millimeters, phi units, and the Wentworth grain size classification is provided in Table **T1.**

Biostratigraphy

Microfossil recovery and preparation

Large microfossils (>63 µm fraction)

A total of 20–25 cm^3 samples from the core catcher and a smaller selection of 5 cm^3 sediment samples submitted from the Petrology group were collected for microfossil analyses. Sediment samples were disaggregated in tap water and washed under flowing water through a nest of sieves with mesh sizes of 1 mm (18 mesh), 150 µm (100 mesh), and 63 µm (230 mesh) until the water passing through the 63 µm (230 mesh) sieve was clean (i.e., the silt-clay fraction had been removed). The immobilized samples (>1 mm, 150 µm–1 mm, and 63–150 µm) were then washed from the sieves using a stream of tap water into Whatman No. 2 filter paper and dried at 100°C for 2 h.

Fossils from each sample/size fraction were screened using a Zeiss Discovery V.12 stereomicroscope. Samples of representative dominant foraminifers from Site C0014 were also selected for examination with a scanning electron microscope (SEM). Samples for SEM examination were hand-picked from a petri plate using a wet toothpick. Samples were then immobilized on an SEM sample holder using double-sided carbon tape for coating and imaging.

Small microfossils (<63 µm fraction)

Smear slides were prepared by first producing an ~10% (v/v) suspension of material from the core catcher samples (i.e., 0.1 cm^3 sediment + 0.9 mL dis-

tilled water in a 1.5 mL microcentrifuge tube). The suspension was allowed to settle for 1 min to sediment sand-sized material at the bottom of the tube, producing a supernatant with a slightly milky consistency. A small drop of this suspension was screened for the presence of coccoliths using phase-contrast light microscopy and cross-polarized light; positive samples were spread across a coverslip and dried using a hot plate for SEM.

Imaging using scanning electron microscopy

Microfossil preparations were Pt coated using a JEOL JFC-1800 nano fine coater and imaged using a JEOL JCM-5700 SEM operating at an accelerating voltage of 5 kV for secondary electron imaging.

Species diversity and abundance

To determine species diversity and species abundance, specimens were identified and counted along a linear axis until ~250 specimens from each group (i.e., foraminifers) were enumerated (where possible). Abundance, preservation, zonal data, and SEM micrographs of dominant or representative taxa for each sample investigated were recorded in the J-CORES database. Foraminifers were identified in relation to the work done by Keller (1980a, 1980b) and Thompson (1980). Coccoliths were identified based on the compilation by Winter and Siesser (1994). Radiolarians were keyed based on the regional work by Sakai (1980).

Petrology

The methodology used during Expedition 331 for visual description of sedimentary and igneous lithological features is outlined in **"Lithostratigraphy"** and will not be repeated here. However, many of the sediments and rocks recovered during Expedition 331 have undergone hydrothermal alteration and/or sulfide mineralization. The procedures used for visually describing these intervals are detailed in the following sections. In addition, this section describes the more advanced petrographic and analytical techniques utilized by the shipboard party to characterize recovered cores, namely X-ray fluorescence (XRF) geochemistry, XRD mineralogy, polished thin section description, and SEM analysis.

Visual description of hydrothermally altered material

During Expedition 331, all rocks logged were graded according to whether they are fresh (<2% by volume alteration products) or have slight (2% to <10%), moderate (10% to <40%), high (40% to <80%), very high (80% to <95%), or complete (95%–100%) alteration. Additionally, through incorporation of VCDs with the results of XRD mineralogical analysis, the style of alteration for each altered interval was determined. A list of alteration styles and their features is given in Table **T2.** Alteration intensity and style were tabulated in Microsoft Excel by core, section, and interval for all holes drilled and included on the section-scale VCDs using Strater software. Symbols used for alteration logging are given in Figure **F4.**

Visual description of sulfides

Seafloor and subseafloor sulfide mineralization can occur as massive sulfides; semimassive sulfides; sulfide minerals in stockwork, stringers, or veins; sulfide filling voids in rocks; sulfide-filled breccia; disseminated sulfides; and metalliferous (sulfide and oxide) sediments (Table **T3**).

Sulfide mineralization styles and sulfide and sulfate mineral species were observed visually and recorded in section-scale templates using the shipboard database software J-CORES. A list of sulfide and sulfate minerals observed during Expedition 331 and their chemical formulas is given in Table **T4.** Visually estimated sulfide abundance was recorded in the written descriptions given for all lithological intervals in J-CORES and then tabulated in Microsoft Excel by core, section, and interval for all holes. Sulfide and sulfate mineral distribution and sulfide abundance were then included on the section-scale VCDs using Strater software. Symbols used for sulfide logging are given in Figure **F4.**

X-ray diffraction

We completed XRD analyses of bulk powders using a PANalytical CubiX PRO (PW3800) diffractometer. Samples were routinely taken from each 1.5 m core section during hydraulic piston coring system (HPCS) and extended shoe coring system (ESCS) drilling and from every second 0.75 m core section for Baker Hughes INTEQ (BHI) cores. Additional samples were selected at irregular intervals where needed to represent the range of lithologies encountered during drilling and provide a more quantitative context for visual core description. Our principal goal was to determine the minerals present in the very fine grained material that made up the bulk of recovery during Expedition 331. Data processing was carried out using X'Pert HighScore Version 2.1 (2.10), which is produced by PANalytical B.V. (Almelo, Netherlands).

X'Pert HighScore matched peaks from the unknown sample to those of known crystal structures from the

Inorganic Crystal Structure Database, which contains thousands of XRD patterns from known synthetic and naturally formed phases. The majority of these reference patterns were gathered from single crystal analyses, which does not allow for the effects of preferred orientation or stacking disorders. These effects can be particularly significant for clay minerals and phyllosilicates. The program therefore provided a guide to potential phases, which were then interpreted by the operator. Interpreted mineralogies were tabulated, in approximate order of abundance, for each sample analyzed and were included in the site reports. Peak heights may be strongly influenced by factors other than abundance, so no quantitative measurement is implied. In particular, abundances of clay and phyllosilicate minerals are not quantitatively estimated and are likely to be underestimated.

Samples were freeze-dried, crushed with a ball mill, and mounted as random bulk powders. Instrument settings were as follows:

Generator = 45 kV and 40 mA.
Tube anode = Cu.
Wavelengths = 1.54060 Å (Kα1) and 1.54443 Å (Kα2).
Step spacing = 0.01°2θ.
Scan step time = 3.000 s.
Divergent slit = automatic.
Irradiated length = 10 mm.
Scanning range = 2°2θ to 60°2θ.
Spinning = yes.

X-ray fluorescence

The lack of technical support for preparation of glass beads and the small size of the core description team for Expedition 331 meant that only four samples were prepared for XRF analysis. Major elements were measured using the fused glass bead method and are presented as weight percent oxide proportions (SiO_2, TiO_2, Al_2O_3, Fe_2O_3, MnO, CaO, MgO, Na_2O, K_2O, and P_2O_5).

An aliquot of 0.9 g of ignited sample powder was fused with 4.5 g of SmeltA12 flux for 7 min at 1150°C to create glass beads. Loss on ignition was measured using weight changes on heating at 1000°C for 3 h. Analyses were performed on the wavelength dispersive XRF spectrometer Supermini (Rigaku) equipped with a 200 W Pd anode X-ray tube at 50 kV and 4 mA. Analytical details and measuring conditions for each component are given in Table **T5.** National Institute of Advanced Industrial Science and Technology (Geological Survey of Japan) rock standards were used as reference materials for quantitative analysis. Table **T6** lists the results and standard deviations for selected standard samples. A calibration curve was created with matrix corrections provided by the operating software, using the average content of each component. Processed data were uploaded into the J-CORES database.

Polished thin section description

The lack of technical support for thin section preparation and the small size of the core description team meant that only six polished thin sections of competent lithologies could be prepared on board the *Chikyu* for microscopic studies of mineralogy, petrology, internal structures, and fabric. A thin section was prepared as a 30 µm (0.03 mm) thick slice of core or cuttings sample. The standard size of billets for thin section preparation was 2 cm × 3 cm × 0.8 cm. Four of the six samples sectioned were strongly altered and porous, so they were dried first in the oven at 105°C and then impregnated under vacuum (Epovac) with epoxy (Epofix) prior to mounting. Polished thin sections were observed in transmitted and reflected light using an Axioskop 40A polarizing microscope (Carl Zeiss) equipped with a Nikon DS-Fi1 digital camera.

Scanning electron microscopy

Aqueous sediment samples were fixed using 2% glutaraldehyde, dehydrated using acetone, and embedded in Epon resin. Friable hard rock samples were embedded directly in Epon to stabilize the material. Nonfriable rock was prepared as conventional polished thin sections. Samples were subsequently ground, polished, and platinum coated using a JEOL JFC-1800 nano fine coater. All samples were viewed on a JEOL 5770 SEM equipped with both backscattering and X-ray spectroscopic (energy-dispersive spectrometry [EDS]) detectors operating at an accelerating voltage of 15 kV.

Geochemistry

Organic geochemistry

Shipboard organic geochemical analyses included volatile hydrocarbon contents (C_1–C_4); inorganic carbon and carbonate contents; and elemental analyses of total carbon, nitrogen, and sulfur. Procedures used generally follow Pimmel and Claypool (2001).

Safety gas monitoring

A 5 cm^3 sediment sample was collected with a cut-off plastic syringe, usually from the exposed end of Section 1, and was extruded into a 20 mL glass vial. The vial was then placed in an oven at 70°C for 30 min. The evolved gases were analyzed using an Agilent

6890N gas chromatograph (GC) equipped with a flame ionization detector (FID). This system determined the concentration of C_1–C_4 hydrocarbons with an FID. Chromatographic response on the GC was calibrated against five different authentic standards with variable quantities of low molecular weight hydrocarbons.

Headspace H_2 and methane (science gas sample)

A 5 cm^3 sediment sample was collected with a cut-off plastic syringe from adjacent to the safety gas sample and as close as possible to the interstitial water sample. The sample was immediately extruded into a 10 mL glass vial containing 3 mL of saturated sodium chloride and one drop of a saturated mercuric chloride solution. The vial was capped with a Teflon-coated butyl rubber stopper. An aliquot of 300–500 µL of headspace gas was drawn from the vial with a plastic syringe and manually injected into a GL Science GC equipped with a helium ionization detector (HID) to determine H_2 and CH_4 concentrations. The GC with HID was supplied by the JAMSTEC SUGAR project as a third-party tool. Chromatographic response on the GC was calibrated against a standard gas mixture (22.7 ppm each of H_2, O_2, N_2, CH_4, and CO).

Inorganic carbon

Inorganic carbon concentrations were determined using a Coulometrics 5012 CO_2 coulometer. About 10–12 mg of vacuum-dried ground sediment was weighed and reacted with 2 M HCl. The liberated CO_2 was titrated, and the change in light transmittance was monitored with a photodetection cell. The weight percentage of calcium carbonate was calculated from the inorganic carbon (IC) content, assuming that all evolved CO_2 was derived from dissolution of calcium carbonate, by the following equation based on molecular weight ratio:

$$CaCO_3\ (wt\%) = 8.33 \times IC\ (wt\%).$$

All carbonate minerals were treated as $CaCO_3$. For Expedition 331, repeated measurements of the NIST SRM 88b (dolomitic limestone) reference material produced a mean IC value of 12.74 ± 0.10 wt%, which corresponds to a $CaCO_3$ composition of 106.1 ± 0.8 wt%.

Elemental analysis

Total carbon, nitrogen, and sulfur concentrations were determined using a Thermo Finnigan Flash EA 1112 CHNS analyzer calibrated using the synthetic standard sulfanilamide, which contains C (41.81 wt%), N (16.27 wt%), and S (18.62 wt%). About 10–20 mg vacuum-dried ground sediment was weighed and placed in a tin container for carbon and nitrogen analyses. For sulfur analysis, the same amount of freeze-dried sediment was weighed and put in a tin container with an equal amount of V_2O_5. Sediment samples were combusted at 1000°C in a stream of oxygen. Nitrogen oxides were reduced to N_2, and the mixture of CO_2, N_2, and SO_2 was separated by GC and detected by a thermal conductivity detector (TCD). Total organic carbon content was calculated by subtraction of inorganic carbon from total carbon. Standard deviation of carbon, nitrogen, and sulfur for the samples is less than ±0.1%.

During Expedition 331, the analytical accuracies of our C and N analyses were confirmed through repeated analyses of Soil NCS reference material, run after every sixth sample, which has a certified composition of 1.755 ± 0.028 wt% for C and 0.195 ± 0.0274 wt% for N. Our observed mean for the Soil NCS reference material was 1.719 ± 0.034 wt% C and 0.1881 ± 0.005 wt% N. The analytical accuracy for our S analyses was determined through repeated analyses of the JMS-1 reference material (from the Geological Society of Japan), run after every sixth sample, which as a certified S composition of 1.32 wt%. Our observed mean for repeated analyses of JMS-1 was 1.23 ± 0.2 wt%. These tests of accuracy include weighing errors.

The reproducibility for the analysis of total carbon (TC) and total nitrogen (TN) when their concentrations were very low was tested using a sample retrieved from Site C0014 (Sample 331-C0014G-17T-4, 40.0–42.0 cm). Repeated analysis of this sample resulted in a mean value of 0.0105 ± 0.0006 wt% (N = 3) for carbon (TC) and 0.0605 ± 0.0008 wt% (N = 3) for nitrogen (TN).

Inorganic geochemistry

Interstitial water collection

We obtained interstitial water typically from 10–20 cm long whole rounds, selected based on core recovery and expedition objectives. Whole rounds were cut and capped, brought into the laboratory, and placed in a nitrogen-filled glove bag, where they were generally scraped to remove contaminated sediment and transferred into a titanium piston-cylinder-type squeezer (Manheim, 1966). The squeezer was removed from the glove bag and placed into a hydraulic press, which was used to compress the sediment to extract the pore water. As the sediment was squeezed, pore water passed through one or two rinsed paper filters mounted on a titanium support

screen and into a plastic syringe. Once collected, the pore water was ejected through a 0.45 µm syringe-mounted filter into plastic bottles or glass vials for various analyses. Where appropriate, these containers were cleaned with HCl and rinsed with 18 MΩ water. Samples for analysis by inductively coupled plasma–optical emission spectrometry (ICP-OES) and inductively coupled plasma–mass spectrometry (ICP-MS) were acidified by adding 4 µL of 6 N HCl per mL sample. We note that precipitation occurred regularly during sample processing both before and after filtering. The precipitate was usually fine grained and black and is probably polymetallic sulfide. Occasionally we also saw white flocs forming in the sampling syringe which may be silica or organics; these flocs did not appear to form following sample filtration. Caution should be exercised in interpreting any data that might be affected by such precipitation.

Interstitial water analysis

Refractive index was measured on a 100 µL filtered aliquot using an RX-5000a refractometer (Atago); this measurement can be used to estimate pore water salinity. pH and alkalinity were measured using a pH electrode and Gran titration with 0.1 M HCl using a Metrohm autotitrator. Chlorinity (Cl + Br) was analyzed by titration with silver nitrate using International Association for the Physical Sciences of the Oceans (IAPSO) seawater as a primary standard. This titration is one of the more precise and accurate chemical measurements we made. For any batch of analyses, no samples were run until the operator achieved a precision of ±0.2% on three consecutive replicates of the IAPSO standard, which was then run frequently throughout the analyses. For 133 replicates of IAPSO run during Expedition 331, we achieved a mean daily precision of 0.4% ± 0.3% (1σ), where the standard deviation represents the variation in the mean precision from day to day.

Sulfate, Br, Mg, Ca, K, and Na were measured using a Dionex ICS-1500 ion chromatograph. Dissolved phosphate, silicon, and ammonium were measured using standard colorimetric methods on a Shimadzu UV-2550 ultraviolet (UV)-visible spectrophotometer. The colorimetric method for Si measures only monomeric silica. We had anticipated measuring Si by ICP-OES shipboard using a Horiba Jobin Yvon Ultima2 ICP-AES, but this instrument was not operational during Expedition 331. Aliquots for Si were not prediluted, so the concentrations we report should be considered minima because of the possibility of polymerization. A preliminary comparison with Si analyses done postcruise by ICP-OES indicates this problem may have been minimal. However, for 10 samples from Site C0014 and all five from Site C0015, ICP-OES yielded lower concentrations than colorimetry in an approximately fixed ratio that likely resulted from either a computational or analytical error. One additional ICP-OES sample from Site C0014, which was part of the group of data that was not used, actually had a higher Si value than the colorimetric analyses. However, the colorimetric analysis of this particular sample is questionable as it was notably low (0.09 mM) compared to the other samples above and below (i.e., >1 mM) and may have suffered from a dilution error. Because of its consistency with other ICP-OES data that appear to suffer from an analytical artifact, we have deleted this value (noted in Table **T8** in Expedition 331 Scientists, 2011a). Although we present both data sets in the site chapter tables, we have removed these 16 ICP-OES analyses, as marked. This error appears to apply only to the Si data. In any case, our interpretations are sufficiently robust that they are unaffected by any remaining inaccuracies in the ICP-OES data.

Because the ICP-OES was not operational during Expedition 331, concentrations of strontium, lithium, iron, manganese, barium, silicon, and boron were determined postcruise, on the *Chikyu*, once the instrument was repaired. Although we used the National Research Council Canada Seawater Reference Materials for Trace Metals—CASS-4 and NASS-5 (North Atlantic Surface Seawater)—as quality controls for these analyses, these standard reference materials have low signal intensities for Ba, Fe, Mn, and Si relative to our samples and thus may not provide a practical assessment of our data quality for these elements. For B, Li, and Sr, the average values we obtained for NASS-5 are 354 ± 8 µM for B, 36.4 ± 3.3 µM for Li, and 73 ± 2 µM for Sr. For CASS-4 the values are 363 ± 15 µM for B, 37 ± 2 µM for Li, and 75 ± 2 µM for Sr. Unfortunately these reference materials do not have certified values for these particular analytes; however, based on their salinity (NASS-5 = 30.4; CASS-4 = 30.7), we would have expected B, Li, and Sr values to be ~370 µM for B, ~23.5 µM for Li, and ~82 µM for Sr for these standards. Data for the elements Zn, Mo, Rb, Cs, and U are reported here and were measured using an Agilent 7500ce ICP-MS equipped with an octopole reaction system and indium internal normalization standard. For quality control we again measured CASS-4 and NASS-5. The average values we obtained for NASS-5 are 80 ± 40 nM for Zn, 97 ± 3 nM for Mo, 1.16 ± 0.03 µM for Rb, 1.81 ± 0.14 nM for Cs, and 10.1 ± 0.8 nM for U. Our average values for CASS-4 are 78 ± 15 nM for Zn, 100 ± 4 nM for Mo, 1.18 ± 0.03 µM for Rb, 1.8 ± 0.2 nM for Cs, and 10.3 ± 0.8 nM for U. These seawater reference materials are not ideal for quality control because our pore waters often differ significantly from

seawater in both major and trace element content. Detection limits are defined as three times the standard deviation of the detection blank determined during the sample runs.

Interstitial waters were analyzed for dissolved inorganic carbon (DIC) on a UIC coulometer (CM5012). These samples were stored at 4°C in 2 mL amber glass vials. For analysis, 500 µL of pore water was placed in a sample vial and purged with N_2 for 1 min to remove headspace gas. After purging, 0.5 mL of 10% phosphoric acid was added to the sample. We used 0.025 and 0.25 M Na_2CO_3 solution (Wako chemical) as standards and analyzed a certified reference material for oceanic CO_2 measurements supplied by Dr. Andrew Dickson of Scripps Institute of Oceanography (San Diego, USA), batch 99, as a quality control solution.

Microbiology

Total prokaryotic cell counts

The abundance of microbial cells in sediments was evaluated using SYBR Green I as a fluorochrome dye with epifluorescence microscopy (Weinbauer et al., 1998). Approximately 0.5 cm^3 of sediment and/or deposit sample was taken with a sterilized spatula. In a clean area of the laboratory, samples were immediately fixed with 4% paraformaldehyde in a phosphate-buffered saline (PBS) buffer and stored at 4°C for 3 h. Fixed samples were diluted with 1× PBS and sonicated for 20 s with an ultrasonic homogenizer UH-50 (SMT, Tokyo, Japan). Microbial cells were directly stained with SYBR Green I (1/2000 [v/v]) at room temperature for 15 min. Cells were then filtered onto a 0.2 µm pore-size membrane filter (GTBP, Millipore). Excess dye was flushed from the membrane by rinsing with a further aliquant of Milli-Q water, and the membrane was mounted for microscopic analysis under glycerol/PBS (1:1) or glycerol using a coverslip. Microbial cells were enumerated with a fluorescence microscope (Axioplan 2, Zeiss) equipped with the fluorescent filter set of 470/20 nm (center wavelength/bandwidth) for excitation and 515 nm for emission.

The lower detection limit to detect one cell depends on the volume put on the filter, the total number of fields, the number of fields of view, and the desired probability to find one cell (Kallmeyer, 2008); the equation is given by

$$n = -T_{fov}/C_{fov} \times \ln(1 - p),$$

where

n = number of cells required,
T_{fov} = microscopic factor (total fields of view),
C_{fov} = counted fields, and
$(1 - p)$ = probability to detect one cell.

The average number of counted fields was 100 fields per sample. To find the optimal balance between the covering of the slide with sediment and detection limit, we varied the volume on the filter and the number of fields slightly during the expedition. Nevertheless, the lower detection limit varied between and 0.65×10^6 and 4.4×10^6 cells/mL sediment because of the limited volume that can be put on the filter by this method (Table **T7**). In some cases, actual cell counts were less than the theoretical detection limit, as the probability to detect one cell was empirically reduced.

Cultivation of thermophiles

Growth of members of *Thermococcales* (e.g., *Thermococcus*), *Aquificales* (e.g., *Persephonella*), thermophilic *Epsilonproteobacteria* (e.g., *Nitratiruptor*), and thermophilic and hydrogenotrophic methanogens (e.g., *Methenothemococcus* and *Methanocaldococcus*) from core samples was used as a biological probe of hydrothermal fluid input in subseafloor environments. Cultivation of *Thermococcales*, *Aquificales*, and thermophilic *Epsilonproteobacteria* was carried out for all regular microbiology samples, whereas enrichment of methanogens was only examined for samples where growth of *Thermococcales*, *Aquificales*, and/or thermophilic *Epsilonproteobacteria* was observed. Media for cultivation of *Thermococcales*, *Aquificales*, thermophilic *Epsilonproteobacteria*, and thermophilic and hydrogenotrophic methanogens were the MJYPS media (Takai et al., 2000), MMJHS media (Takai et al., 2003), and MMJ media (Takai et al., 2002), respectively. N_2 was used as the headspace gas for the MJYPS media, and a mixture of 80% H_2 and 20% CO_2 (2 atm) was used for the MMJHS and MMJ media. Incubation temperatures for the MJYPS, MMJHS, and MMJ media were 80°C, 55°C, and 55°C and 70°C, respectively.

Additional cultivation of *Thermococcus* was conducted using the same method as described in Holden et al. (2001) with YPS media in 10 mL Balch tubes using headspace flushed with argon at both 80°C and 90°C.

Cultivation of sulfate reducers

Sediment slurries from a variety of layers were cultivated to isolate sulfate-utilizing bacteria and to determine if they were capable of using methyl sulfides as a substrate. Artificial seawater (Lyimo et al., 2002) (15 mL) with 0.1 g/L of sodium sulfide was placed in gas-tight 50 mL tubes and autoclaved under 80% N_2

and 20% CO_2 (0.5 atm). Substrates for sulfate reducers were added later, prior to inoculation. A total of four types of media were prepared:

- Two types of substrate mixture with/without 25 mM bromoethanesulfonic acid (BES), which is an inhibitor of methanogenic archaea;
- A mixture of dimethyl sulfide (DMS) and methyl mercaptan (MeSH) at concentrations of 10 µM and 11 µM, respectively, following Lyimo et al. (2009); and
- A mixture of lactate and acetate (1.25 µM each).

Sediment slurry for each section was inoculated in these four types of media, and tubes were incubated at temperatures similar to downhole conditions.

Cultivation of iron-oxidizing bacteria

Sediment slurry was also used for the onboard cultivation of iron-oxidizing bacteria (FeOB). We used essentially the same protocol as described in Emerson and Floyd (2005), using two types of media:

1. A modified artificial seawater (ASW) media with 5 mM MES (pH 6.5), minerals, and zero valence iron (Fe^0) and
2. A modified ASW media with 5 mM sodium nitrate, 5 mM MES (pH 6.5), minerals, and Fe^0.

The first media (without sodium nitrate) is referred to as ASW media A. The second media (with sodium nitrate) is referred to as ASW media B. All samples inoculated in ASW media A were incubated at room temperature in a microaerophilic environment using a CampyPak microaerophilic system in an anaerobic (i.e., gas-tight) jar. All samples inoculated in ASW media B were incubated at room temperature in an anaerobic environment using a GasPak anaerobic system in an anaerobic jar. Samples were incubated for 3–6 days, after which growth was assessed using epifluorescence microscopy with either a SYTO 13 or SYBR Green I nucleic acid stain. For successful samples, between 0.02 and 0.5 mL was also fixed with one drop 50% glutaraldehyde overnight, washed with sterile water, and dried at room temperature before being imaged using the onboard SEM and analyzed by X-ray EDS. Subsamples of successful enrichments were stored both with and without 10% glycerol in ASW media A; both were subsequently fast frozen in liquid nitrogen and stored at –80°C for future shore-based analyses.

Contamination test

Fluorescent microspheres were used for contamination assessment of each HPCS core from which microbiology samples were taken following standard IODP procedures (Smith et al., 2000). Perfluorocarbon tracer (PFT) (perfluoromethylcyclohexane; MW = 350.6; Matrix Scientific, USA) was also applied for contamination assessment as a chemical tracer for all coring systems. When drill mud components were solved in surface seawater, PFT was added to the drill mud tank. The concentration of PFT in the drilling fluid was monitored after PFT was added (Table **T8**). In addition, potential maximum PFT concentrations in the drill hole were monitored from adhered mud on a cored rock surface from Site C0016 (see Table **T6** in Expedition 331 Scientists, 2011b). Quantification of PFT in core samples and original drilling mud fluids was carried out following standard IODP procedures (Smith et al., 2000) and using an Agilent Technologies model 6890N gas chromatograph (GC) with an electron capture detector (ECD) (Agilent Technologies). The GC was equipped with an HP-PLOT Al_2O_3 "M" deactivation column (length = 30 m; inside diameter = 0.53 mm; coating thickness = 15 µm). Helium and nitrogen were used as the carrier gas and make-up gas, respectively.

Physical properties

Continuous physical property measurements provide basic information through nondestructive means to assist characterization of lithological units and states of consolidation and deformation. For all core sections, X-ray CT images were captured first, followed by automated measurement of GRA density, *P*-wave velocity (PWV), and noncontact electrical resistivity using a MSCL-W. Cores were allowed to thermally equilibrate at room temperature, ~20°C (Expedition 315 Scientists, 2009; Expedition 316 Scientists, 2009), prior to these measurements. After MSCL-W measurements, thermal conductivity measurements were carried out on whole-round core sections for soft sediments and on the working half of split cores for hard sediments and rocks. Thermal conductivity was usually measured using a full-space needle probe method on soft sediments. In rare cases, we used a half-space line source probe method on split working halves because the sediments were lithified and could not be penetrated with the needle probe. Digital photo image scanning and color spectrophotometry were carried out on the split surfaces of archive halves using the MSCL-I and the MSCL color spectrophotometer (MSCL-C), respectively (Expedition 315 Scientists, 2009; Expedition 316 Scientists, 2009). MAD measurements were made on discrete samples collected from working halves; in general, discrete samples were taken once per section, and when possible, samples were taken from both above and below the whole rounds collected for microbiological and interstitial water sam-

pling. Discrete measures of formation factor were determined from electrical resistivity (impedance) in working halves at two to three positions within each section. Discrete PWV measurements were conducted in three orthogonal directions in 20 mm cubic samples collected in lithified sediments. Details about each measurement are given in the following sections.

Multisensor core logger for whole-round samples

Gamma ray attenuation density

A thin gamma ray beam was produced by a ^{137}Cs gamma ray source at a radiation level of 370 MBq within a lead shield with a 5 mm collimator. The gamma ray detector consisted of a scintillator and an integral photomultiplier tube. Calculation of bulk density from gamma ray attenuation utilized the following equation:

$$\rho = 1/(\mu \times d) \times \ln(I_o/I),$$

where

- ρ = sediment bulk density,
- μ = Compton attenuation coefficient,
- d = sample thickness,
- I_o = gamma source intensity, and
- I = measured intensity through the sample.

Because μ and I_o are treated as constants, ρ can be calculated from I. We used a set of aligned aluminum cylinders of various thicknesses surrounded by distilled water in a sealed core liner for calibration. Gamma counts were taken through each cylinder (count time = 60 s), and $\ln(I)$ was plotted against ($\rho \times d$). The density (ρ) of each aluminum cylinder was 2.7 g/cm^3, and d was 1, 2, 3, 4, 5, or 6 cm. The relationship between I and ($\rho \times d$) can be expressed as follows:

$$\ln(I) = A(\rho \times d)^2 + B(\rho \times d) + C,$$

where A, B, and C are coefficients determined during calibration. The MSCL provided the values of I and d, and ρ was calculated with the equation above. This density measurement was conducted every 4 cm for a duration of 4 s. The spatial resolution of the measurement was 5 mm, so each data point reflects the properties of the closest 5 mm interval.

Porosity (ϕ) is calculated from MSCL density assuming a solid grain density (ρ_s) of 2.7 g/cm^3 and a pore fluid density (ρ_f) of 1.024 g/cm^3:

$$\phi = (\rho_s - \rho)/(\rho_s - \rho_f).$$

P-wave velocity

The basic relationship for sonic velocity is

$$v = d/t,$$

where

- d = distance traveled through the core and
- t = traveltime though the core.

PWV transducers are mounted on the MSCL system and measure d and t horizontally throughout the entire core. Total traveltime measured between the transducers includes three types of correctable "delay":

1. t_{delay} = delay related to transducer faces and electronic circuitry,
2. t_{pulse} = delay related to the peak detection procedure, and
3. t_{liner} = transit time through the core liner.

The effects of delays are calibrated using a core liner filled with pure water. For routine measurements on whole rounds in core liners,

$$v_{core} = (d'_{core} - 2d_{liner})/(t_0 - t_{pulse} - t_{delay} - 2t_{liner}) \times 1000,$$

where

- v_{core} = corrected velocity through core (km/s),
- d'_{core} = measured diameter of core and liner (mm),
- d_{liner} = liner wall thickness (mm), and
- t_0 = measured total traveltime (µs).

Because of issues with reconfiguration of the MSCL-W for 4 inch diameter core sections, PWV measurements were not undertaken for cores taken with the BHI industry-standard coring system. This only applies to Core 331-C0013E-7L and all cores from Hole C0016B.

Electrical resistivity

The bulk electrical resistivity (R_e) of a core of length (L) and cross-sectional area (S) at constant temperature can be expressed as

$$R_e = R(S/L),$$

where R is electrical resistance. The bulk resistivity of sediments and rocks is lower than that of the rock matrix because of the presence of relatively high conductivity fluids.

The noncontact resistivity sensor on the MSCL system operates by inducing a high-frequency magnetic field in the core from a transmitter coil, which in turn induces electrical currents in the core that are inversely proportional to the resistivity. Very small magnetic fields generated by the electrical current are measured by a receiver coil. To measure these

magnetic fields accurately, a different technique has been developed that compares readings generated from the measuring coils to readings from an identical set of coils operating in air. Electrical resistivity data were obtained at 4 cm intervals.

Thermal conductivity

Thermal conductivity measurements were conducted on whole rounds using a needle probe method (VLQ probe) and/or on split cores using a half-space method (HLQ probe) and a TeKa TK04 thermal conductivity meter.

The TK04 determines thermal conductivity based on a transient heat flow method. The heating wire and a temperature sensor are incorporated in a needle probe. When the wire is heated, the surface temperature of the probe is recorded simultaneously. The thermal conductivity of the surrounding material can be calculated from the temperature versus time measurement curve based on the simple calculation of the thermal conductivity coefficient:

$$k_a(t) = (q/4\pi)\{[\ln(t_2) - \ln(t_1)]/[T(t_2) - T(t_1)]\},$$

where

q = heat input per unit length and unit time,
$k_a(t)$ = apparent thermal conductivity,
t_1, t_2 = picking times, and
$T(t_1)$, $T(t_2)$ = corresponding source temperatures.

Because $k_a(t)$ is not constant but depends on the time interval used for calculation of thermal conductivity, the real thermal conductivity is approached only for sufficiently large heating times. A special approximation method in the TK04 software automatically detects disturbances and determines the optimal time interval of the heating curve for evaluation. Heating power and evaluation parameters are changed depending on the specific sample.

In general, thermal conductivity measurements are made twice in each core section. For whole-round cores, a small hole was drilled in the core liner, usually ~26 and ~100 cm from the top of each section. A 2 mm diameter temperature probe (VLQ) was inserted into the working half of the core section. At the beginning of each measurement, temperature in the samples was monitored automatically without applying a heater current until the background thermal drift was determined to be <0.2 mK/h. The heater circuit closed automatically, and the temperature increase in the probe was recorded.

For cores that were too consolidated to permit use of the needle probe, we used a half-space method measurement. Briefly, an ~10 cm long split-core piece was taken from the working half of the core and placed in seawater at ambient temperature (20°C) for 15 min. The HLQ probe was placed on a flat surface of the sample with the line probe oriented parallel to the core axis, and heating and measurements were conducted automatically. The core and the probe were placed in an insulating cooler, wrapped in a soft cloth, and covered with a piece of bubble-wrap to maintain the ambient temperature. The measurement of temperature drift and conductivity was conducted in the same way as with the VLQ probe.

During each 24 h period, the TK04 was calibrated using standard blocks that have nominal conductivities of 1.623 W/(m·K) ± 2% for the VLQ probe and 1.652 W/(m·K) ± 2% for the HLQ probe, respectively. Measurements for the standard blocks were then plotted against the true values, and the slope of the linear regression obtained was used to calibrate core sample measurements.

Moisture and density

MAD measurements on rocks and sediments were calculated by measuring wet mass, dry mass, and dry volume.

Core samples

Discrete samples of ~5–7 cm^3 were taken for each measurement at a spacing of approximately one sample per each working-half section. In addition, for those sections where whole rounds were removed for microbiological and interstitial water sampling, MAD samples were routinely taken both above and below (i.e., "bracketing") the whole-round sample. In general, care was taken to sample undisturbed parts of the core and to avoid drilling mud. In soft sediments, samples were collected using a cut-off 10 cm^3 syringe as a small piston core. When present, hard sediments and rock samples were cut into 2 cm × 2 cm × 2 cm cubes with a parallel-blade rock saw and then soaked for 6 h in a 35 ppt NaCl solution prior to MAD measurements. Immediately after the samples were collected, wet sediment mass (M_w) was measured. Dry sediment mass (M_d) and dry volume (V_d) were measured at room temperature after drying the sample in a convection oven for 24 h at 105° ± 5°C and cooling the sample for 1 h in a room-temperature desiccator. Wet and dry masses were determined by weighing using a custom-built BAL-2 motion-compensated shipboard system of paired electronic balances that compensate for the ship's heave. The sample mass was counterbalanced with a precisely known mass (usually 10 g) that was within 5 g of the sample mass. The sample mass was determined to a precision of at least ±0.01 g (generally better). The balance system was calibrated once each

day. Dry volume was measured using a helium-displacement pycnometer (Quantachrome pentapycnometer) with a nominal precision of ±0.04 cm^3. Volume measurements were repeated a minimum of three and up to five times until the standard deviation of the average volume was within ±0.2%. A reference volume (calibrated sphere) was run with each group of four samples, and the sphere was rotated between cells to check for systematic error.

Bulk density, dry density, and density of the solids, as well as porosity and moisture content (void ratio), were computed, taking into account the precipitation of dissolved salts during drying using traditional IODP methods (Method C; Blum, 1997). Water content, porosity, and void ratio are defined by the mass (or volume) of extracted water before and after removal of all water present in the sample through the drying process. This includes interstitial water (inside the pores) as well as water sorbed to hydrous minerals. Standard seawater density (ρ_w = 1.025 g/cm^3) is assumed for pore fluid density.

Mass of water, mass of salt, volume of water, and water content

Pore water mass (M_w), mass of salt (M_s), pore water volume (V_{pw}), and salt volume (V_s) can be calculated by

$$M_w = (M_t - M_d)/(1 - s),$$

$$M_s = M_w - (M_t - M_d) = (M_t - M_d) \times s/(1 - s),$$

$$V_{pw} = M_w/\rho_w = (M_t - M_d)/[(1 - s) \times \rho_w],$$

and

$$V_s = M_s/\rho_s = [(M_t - M_d) \times s/[(1 - s)]/\rho_s],$$

where

M_t = total mass of the saturated sample (grams),
M_d = dry mass of the sample (grams),
s = permil salinity (s = 35‰), and
ρ_s = density of salt (2.257 g/cm^3).

Bulk density

Bulk density (ρ) is the density of the saturated samples defined as

$$\rho = M_t/V_t.$$

Bulk mass (M_t) is measured with the balance, and bulk volume (V_t) is determined from the pycnometer measurement of dry volume (V_d) and the calculated volumes of pore fluid and salt ($V_t = V_{pw} + V_d$).

Porosity

Porosity (ϕ) was calculated using

$$\phi = [(1 + W_c) \times \rho_w]/(W_c \times \rho) = V_{pw}/V_t$$

where

ρ = measured bulk density,
ρ_w = density of the pore fluid, and
W_c = water content expressed as a decimal ratio of percent dry weight.

Grain density

Grain density (ρ_{grain}) was determined from measurements of dry mass and dry volume made in the balance and in the pycnometer, respectively. Mass and volume were corrected for salt using

$$\rho_{grain} = (M_d - M_s)/[V_d - (M_s/\rho_{salt})],$$

where

M_s = salt content (grams) and
ρ_{salt} = density of salt (2.257 g/cm^3).

Water content

Water content (W_c) was determined following the methods of the American Society for Testing and Materials (ASTM) designation D2216 (ASTM International, 1990). Corrections are required for salt when measuring the water content of marine samples. In addition to the recommended water content calculation in ASTM D2216 (i.e., the ratio of pore fluid mass to dry sediment mass, percent dry weight [% dry wt]), we also calculated the ratio of pore fluid mass to total sample mass (percent wet weight [% wet wt]). The equations for water content are

$$W_c \text{ (\% dry wt)} = (M_t - M_d)/[M_d - (s \times M_t)]$$

and

$$W_c \text{ (\% wet wt)} = (M_t - M_d) \times [(1 + s)/M_t],$$

where

M_t = total mass (in grams) of the saturated sample,
M_d = mass (in grams) of the dried sample, and
s = permil salinity (‰).

Discrete measurement of formation factor (electrical resistivity)

In addition to bulk resistivity measurements from the MSCL-W, discrete measurements of electrical resistivity were made in order to calculate formation factor. The effect of pore fluid on bulk resistivity depends on whether the fluid-filled pores are con-

nected. The bulk electrical resistivity of a fluid-filled sediment (R_e) relative to that of the pore fluid (R_f) alone is described by an apparent formation factor F_a (Archie, 1947):

$$F_a = R_e/R_f.$$

The formation factor is correlated with pore structure within the core (porosity, permeability, tortuosity, and so on). Values of F_a include the effect of grain-surface conductivity and thus do not represent the true formation factor,

$$F = \tau^2/\phi_c,$$

where

τ = true tortuosity of the fluid flow path and
ϕ_c = connected porosity.

Resistivity of pore water and sediment (R_f and R_e, respectively) is calculated from the measured absolute impedance ($|Z|$) and phase angle (Θ):

$$R = |Z| \times \cos\Theta.$$

In practice, we assume that pore water has the same resistivity as seawater and record the resistivity of a 35‰ NaCl solution rather than the resistivity of the pore water.

Equipment

Electrical resistivity was measured in working-half cores using a home-built electrode and an Agilent 4294 impedance analyzer. This system was developed onboard the *Chikyu*. The two terminal electrodes comprise two aluminum plates separated by an acrylic block (plates are 1 cm × 2 cm in area, with 2 cm clearance between the electrodes; this yields an electrode constant of 0.02 Ωm). Calibration of the system was performed once each day and consists of measuring the upper and lower resistivity ranges. The upper range (i.e., infinite resistivity) is measured with the two electrodes spaced 2 cm apart in air; the lower range (i.e., the short-circuit condition) is measured with the electrodes touching each other (pinched together by hand). This is followed by measurement of a 35‰ NaCl solution as a quality control check. The NaCl solution measurement should be done once per day or more frequently if the measurement is drifting unacceptably. The voltage and current signal levels for the impedance analyzer are 500 mV and 20 mA, respectively. The alternating-current frequency is swept from 40 to 110 MHz. The measurement of impedance is frequency dependent because there are polarization effects. Phase angles for both the NaCl solution and sediments have been empirically determined to be nearly zero between 10 and 1000 kHz; we record impedance data at a frequency of 100 kHz.

Measurements in sediments and seawater

For split cores, electrodes are placed into the sediment with the 2 cm opening aligned to the long axis of the core in order to minimize edge effects. Impedance and phase angle are recorded after approximately three scans to ensure signal stability. These planar electrodes are only suitable for relatively soft sediments. If the sediments crack upon insertion of the electrodes, the measured impedance will reflect an artificially high resistivity due to air-filled void spaces introduced upon cracking. Measurements were not made when sediments cracked upon electrode insertion. The *Chikyu* does not yet have a needle-type electrode system that will work in more consolidated sediments. Impedance measurements were made at least once per section (minimally at the depths corresponding to the thermal conductivity and MAD measurements) and generally, assuming good recovery, at two to three positions in each section. Care was taken not to disturb a significant portion of the sediment during the measurement.

For NaCl reference solution measurements, the same electrode was used. The electrode was cleaned with distilled water and placed in a beaker of 35‰ NaCl. The electrode was lowered into the solution just to the depth of the acrylic spacer to ensure the water was measured in the same geometric configuration as in the cores.

Discrete measurements of *P*-wave velocity and anisotropy

PWV was measured on discrete samples taken from cores at a sampling frequency of roughly one per section. Core pieces were cut with a rock saw equipped with two parallel blades spaced 20 mm apart. This sample preparation enables measurement of *P*-wave anisotropies in three orthogonal directions. All cubes were cut with faces orthogonal to the *x*-, *y*-, and *z*-axes of the core reference and were soaked in a 35‰ NaCl solution for 6 h prior to analysis. Orientation of the axes is defined as the *z*-axis pointing down the core axis, the *x*-axis pointing into the working half, and the *y*-axis pointing along the core face.

A newly installed *P*-wave logger for discrete samples (PWL-D) was used (Geotek LTD, London, UK). Its basic measurement principle is to measure *P*-wave traveltime and sample length and then calculate PWV. To measure PWV along a given direction, the sample is held by two 1.5 kg weights with a force of ~30 N (corresponding to a pressure of 75 kPa) between two

transducers covered with rubber spacers to ensure good contact between the sample and the transducers. Both the transmitter and receiver are a type of Piezo-composite transducer, and the frequency of the compressible wave (*P*-wave) generated by the transmitter is 230 kHz. The transmitter is connected to a pulse generator; the receiver is connected to an amplifier, and the received signal is processed through an analog-to-digital converter (and then displayed on a PC). The traveltime is picked and logged automatically based on a threshold set by the operator. The sample dimension in the *P*-wave path is automatically measured at the same time as the traveltime measurement by a distance laser sensor mounted in the apparatus.

Quality control checks are conducted daily using a glass sample and an acrylic sample. Calibrations of traveltime and laser distance sensor corrections were conducted only when quality control checks failed to meet designated specifications. The traveltime offset was determined by placing the transmitter and the receiver in direct contact and measuring traveltime. This setup has a time offset of ~9.8 ms. The offset is subtracted from the total traveltime to obtain the true traveltime through the sample. The velocity along a given direction is given by the sample dimension divided by the traveltime. Laser distance calibration was made by placing the transmitter and the receiver in direct contact (zero distance) and then spacing the transducers with a brass reference piece of 2.5 cm height.

P-wave velocity anisotropy

Three directional measurements on discrete samples for PWV were performed on hard sediment and rock samples. Core pieces were cut with a saw equipped with two parallel disks spaced 20 mm apart. If the core has no (or subhorizontal) apparent stratification or foliation, cubes are cut with faces 1, 2, and 3 orthogonal to the *x*-, *y*- and *z*-axes of the core reference, respectively. Orientation of the axes is the same as for paleomagnetism, with the *z*-axis pointing down along the core axis, the *x*-axis pointing into the working half, and the *y*-axis pointing along the core face.

In situ temperature measurements

In situ temperature measurements were made using the APCT3 tool in conjunction with the HPCS. The APCT3 consists of three components: electronics, coring hardware, and computer software. During Expedition 331, in situ temperature measurements were attempted at Sites C0013, C0014, and C0017 during HPCS coring. Temperature sensors were calibrated for a working range of 0° to 50°C, and the instrument can measure a maximum temperature of 55°C.

Prior to entering the hole, the instrument was held at the approximate mudline for ~5 min to thermally equilibrate with the bottom water. This step provides both a clear time-series initiation point and a more accurate bottom water temperature from which to determine relative downhole temperature changes. Because the core winch depth meter was not calibrated, site-to-site variability in the measured bottom water temperature is likely due to uncertainties in depth. After equilibration, the tool was lowered down the hole and penetrated the formation, causing a rise in temperature due to frictional heating. Following the initial rise in temperature, measured temperatures decreased along a decay curve to near equilibrium. During this decay phase, it is important that the temperature tool is not disturbed; thus, drilling was halted for ~5 min to record temperatures. A second rise in temperature is due to frictional heating as the tool is pulled out of the formation. Temperature was measured as a time series sampled once per second and logged to a microprocessor within the downhole tool; when the tool was retrieved, data were downloaded to a computer. The formation equilibrium temperature is determined based on fitting the temperature decay curve using the program TP-Fit, which runs on Matlab (M. Heeseman, pers. comm., 2007).

Determination of heat flow

If heat transfer is by conduction and heat flow is constant, the thermal gradient will be inversely proportional to thermal conductivity, according to Fourier's law. This relationship can be linearized by plotting temperature as a function of summed thermal resistance (Bullard, 1939).

If summed thermal resistance is

$$\sum_{i=1}^{N} \left(\frac{\Delta z_i}{k(z)_i} \right),$$

where

z = depth,

then

$$T(z) = T_0 + q \sum_{i=1}^{N} \left(\frac{\Delta z_i}{k(z)_i} \right)$$

where

T = temperature,
z = depth,
T_0 = bottom water temperature,
q = heat flow, and

N = number of thermal conductivity measurements.

In practice, q and T_0 are estimated by plotting $T(z)$ against summed thermal resistance.

Multisensor core logger imaging system

The MSCL-I scans the surface of archive-half cores and creates a digital image. The line-scan camera is equipped with three charge-coupled devices (CCDs), each with 1024 arrays. Light reflection from the sample surface passes through the lens and is split into three paths (red, green, and blue) by a beam splitter inside the line-scan camera. Each reflection is then detected by the corresponding CCD. Finally, the signals are recombined to produce a digital image. Optical distortion downcore is prevented by precise movement of the camera. Spatial resolution is 100 pixels/cm.

Multisensor core logger color spectroscopy logger

A color spectrophotometer (Konica-Minolta, CM-2600d) is included on the MSCL-C system. The x-y-z type aluminum frame allows operators to set a maximum of seven core sections on the tray, and the sensor unit (including the spectrophotometer and small distance measuring system using a laser sensor) moves across each section and is lowered at each measurement point to measure the split archive core surface.

Light reflected from the sample surface is collected in the color spectrophotometer's integration sphere. The instrument's structure allows for the specular component to be included (SCI setting) or excluded (SCE setting). The SCE setting is the recommended mode of operation, especially for sediments, in order to exclude glare. The light is then divided into wavelengths at a 10 nm pitch (400–700 nm), and the spectral sensors in the sphere convert the light to an electrical current proportional to the intensity of the light. Next, the color spectrum from the sample is normalized by the source light of the reflectance. The spectrum obtained is calibrated based on the measurement of a pure white (high) standard and a black box (zero) standard. The pure white standard has a high reflectance true value at visible wavelengths and is measured by the vendor. Measurements can be calculated based on the 2° or 10° standard observer and any of 11 illuminants. Color reflectance is categorized as an IODP standard measurement, and the measured color spectrum is normally converted to L*, a*, and b* parameters. L*, a*, and b* provide relative changes in the composition of the bulk material and are widely used to correlate sections from core-to-core or hole-to-hole and to analyze the characteristics and cyclicity of lithological changes.

References

Archie, G.E., 1947. Electrical resistivity—an aid in core analysis interpretation. *AAPG Bull.,* 31(2):350–366.

ASTM International, 1990. Standard method for laboratory determination of water (moisture) content of soil and rock (Standard D2216–90). In *Annual Book of ASTM Standards for Soil and Rock* (Vol. 04.08): Philadelphia (Am. Soc. Testing Mater.). [revision of D2216-63, D2216-80]

Blum, P., 1997. Physical properties handbook: a guide to the shipboard measurement of physical properties of deep-sea cores. *ODP Tech. Note,* 26. **doi:10.2973/odp.tn.26.1997**

Bullard, E.C., 1939. Heat flow in South Africa. *Proc. R. Soc. London, Ser. A,* 173(955):474–502. **doi:10.1098/rspa.1939.0159**

Emerson, D., and Floyd, M.M., 2005. Enrichment and isolation of iron-oxidizing bacteria at neutral pH. *Methods Enzymol.,* 397:112–123. **doi:10.1016/S0076-6879(05)97006-7**

Expedition 315 Scientists, 2009. Expedition 315 methods. *In* Kinoshita, M., Tobin, H., Ashi, J., Kimura, G., Lallemant, S., Screaton, E.J., Curewitz, D., Masago, H., Moe, K.T., and the Expedition 314/315/316 Scientists, *Proc. IODP,* 314/315/316: Washington, DC (Integrated Ocean Drilling Program Management International, Inc.). **doi:10.2204/iodp.proc.314315316.123.2009**

Expedition 316 Scientists, 2009. Expedition 316 methods. *In* Kinoshita, M., Tobin, H., Ashi, J., Kimura, G., Lallemant, S., Screaton, E.J., Curewitz, D., Masago, H., Moe, K.T., and the Expedition 314/315/316 Scientists, *Proc. IODP,* 314/315/316: Washington, DC (Integrated Ocean Drilling Program Management International, Inc.). **doi:10.2204/iodp.proc.314315316.132.2009**

Expedition 331 Scientists, 2011a. Site C0014. *In* Takai, K., Mottl, M.J., Nielsen, S.H., and the Expedition 331 Scientists, *Proc. IODP,* 331: Tokyo (Integrated Ocean Drilling Program Management International, Inc.). **doi:10.2204/iodp.proc.331.104.2011**

Expedition 331 Scientists, 2011b. Site C0016. *In* Takai, K., Mottl, M.J., Nielsen, S.H., and the Expedition 331 Scientists, *Proc. IODP,* 331: Tokyo (Integrated Ocean Drilling Program Management International, Inc.). **doi:10.2204/iodp.proc.331.106.2011**

GE Healthcare, 2006. *LightSpeed Series Learning and Reference Guide-Multi Slice CT:* Waukesha, Wisconsin (GE Healthcare), 936.

Holden, J.F., Takai, K., Summit, M., Bolton, S., Zyskowski, J., and Baross, J.A., 2001. Diversity among three novel groups of hyperthermophilic deep-sea *Thermococcus* species from three sites in the northeastern Pacific Ocean. *FEMS Microbiol. Ecol.,* 36(1):51–60. **doi:10.1111/j.1574-6941.2001.tb00825.x**

Kallmeyer, J., Smith, D.C., Spivack, A.J., and D'Hondt, S., 2008. New cell extraction procedure applied to deep subsurface sediments. *Limnol. Oceanogr.: Methods,* 6:236–245. **http://www.aslo.org/lomethods/free/2008/0236.pdf**

Keller, G., 1980a. Benthic foraminifers and paleobathymetry of the Japan Trench area, Leg 57, Deep Sea Drilling Project. *In* Scientific Party, *Init. Repts. DSDP,* 56, 57: Washington, DC (U.S. Govt. Printing Office), 835–865. **doi:10.2973/dsdp.proc.5657.124.1980**

Keller, G., 1980b. Planktonic foraminiferal biostratigraphy and paleoceanography of the Japan trench, Leg 57, Deep Sea Drilling Project. *In* von Huene, R., Nasu, N., et al., *Init. Repts. DSDP,* 56, 57: Washington, DC (U.S. Govt. Printing Office), 809–833. **doi:10.2973/dsdp.proc.5657.123.1980**

Lyimo, T.J., Pol, A., Harhangi, H.R., Jetten, M.S.M., and Op den Camp, H.J.M., 2009. Anaerobic oxidation of dimethylsulfide and methanethiol in mangrove sediments is dominated by sulfate-reducing bacteria. *FEMS Microbiol. Ecol.*, 70(3):483–492. **doi:10.1111/j.1574-6941.2009.00765.x**

Lyimo, T.J., Pol, A., and Op den Camp, H.J.M., 2002. Sulfate reduction and methanogenesis in sediments of Mtoni Mangrove Forest, Tanzania. *Ambio*, 31(7):614–616. **doi:10.1579/0044-7447-31.7.614**

Manheim, F.T., 1966. A hydraulic squeezer for obtaining interstitial waters from consolidated and unconsolidated sediments. *Geol. Surv. Prof. Pap. (U. S.),* 550-C:256–261.

Mazzullo, J., and Graham, A.G. (Eds.), 1988. Handbook for shipboard sedimentologists. *ODP Tech. Note,* 8. **doi:10.2973/odp.tn.8.1988**

Mazzullo, J.M., Meyer, A., and Kidd, R.B., 1988. New sediment classification scheme for the Ocean Drilling Program. *In* Mazzullo, J.M., and Graham, A.G. (Eds.), *Handbook for shipboard sedimentologists*. ODP Tech. Note, 8:45–67. **doi:10.2973/odp.tn.8.1988**

McCave, I.N., Manighetti, B., and Robinson, S.G., 1995. Sortable silt and fine sediment size/composition slicing: parameters for palaeocurrent speed and palaeoceanography. *Paleoceanography,* 10(3):593–610. **doi:10.1029/94PA03039**

Mees, F., Swennen, R., Van Geet, M., and Jacobs, P., 2003. Applications of X-ray computed tomography in the geosciences. *Geol. Soc. Spec. Publ.,* 215(1):1–6. **doi:10.1144/GSL.SP.2003.215.01.01**

Nakano, T., Nakashima, Y., Nakamura, K., and Ikeda, S., 2000. Observation and analysis of internal structure of rock using X-ray CT. *Chishitsugaku Zasshi,* 106(5):363–378.

Paull, C.K., Hills, S.J., and Thierstein, H.R., 1988. Progressive dissolution of fine carbonate particles in pelagic sediments. *Mar. Geol.,* 81(1–4):27–40. **doi:10.1016/0025-3227(88)90015-1**

Pimmel, A., and Claypool, G., 2001. Introduction to shipboard organic geochemistry on the *JOIDES Resolution. ODP Tech. Note,* 30. **doi:10.2973/odp.tn.30.2001**

Ramaswamy, V., and Rao, P.S., 2006. Grain size analysis of sediments from the northern Andaman Sea: comparison of laser diffraction and sieve-pipette techniques. *J. Coastal Res.,* 224:1000–10009. **doi:10.2112/04-0162.1**

Sakai, T., 1980. Radiolarians from Sites 434, 435, and 436, Northwest Pacific, Leg 56, Deep Sea Drilling Project. *In* von Huene, R., Nasu, N., et al., *Init. Repts. DSDP,* 56, 57: Washington, DC (U.S. Govt. Printing Office), 695–733. **doi:10.2973/dsdp.proc.5657.119.1980**

Shepard, F.P., 1954. Nomenclature based on sand-silt-clay ratios. *J. Sediment. Petrol.,* 24(3):151–158. **http://jsedres.sepmonline.org/cgi/reprint/24/3/151.pdf**

Smith, D.C., Spivack, A.J., Fisk, M.R., Haveman, S.A., and Staudigel, H., 2000. Tracer-based estimates of drilling-induced microbial contamination of deep sea crust. *Geomicrobiol. J.,* 17(3):207–219. **doi:10.1080/01490450050121170**

Stuut, J.-B.W., Prins, M.A., Schneider, R.R., Weltje, G.J., Jansen, F.J.H., and Postma, G., 2002. A 300-kyr record of aridity and wind strength in southwestern Africa: inferences from grain-size distributions of sediments on Walvis Ridge, SE Atlantic. *Mar. Geol.,* 180(1–4):221–233. **doi:10.1016/S0025-3227(01)00215-8**

Syvitski, J.P.M. (Ed.), 1991. *Principles, Methods, and Application of Particle Size Analysis*: Cambridge (Cambridge Univ. Press).

Takai, K., Inagaki, F., Nakagawa, S., Hirayama, H., Nunoura, T., Sako, Y., Nealson, K.H., and Horikoshi, K., 2003. Isolation and phylogenetic diversity of members of previously uncultivated ε-Proteobacteria in deep-sea hydrothermal fields. *FEMS Microbiol. Lett.,* 218(1):167–174. **doi:10.1111/j.1574-6968.2003.tb11514.x**

Takai, K., Inoue, A., and Horikoshi, K., 2002. *Methanothermococcus okinawensis* sp. nov., a thermophilic, methane-producing archaeon isolated from a Western Pacific deep-sea hydrothermal vent system. *Int. J. Syst. Evol. Microbiol.*, 52(4):1089–1095. **doi:10.1099/ijs.0.02106-0**

Takai, K., Sugai, A., Itoh, T., and Horikoshi, K., 2000. *Palaeococcus ferrophilus* gen. nov., sp. nov., a barophilic, hyperthermophilic archaeon from a deep-sea hydrothermal vent chimney. *Int. J. Syst. Evol. Microbiol.*, 50(2):489–500. **http://ijs.sgmjournals.org/cgi/content/abstract/50/2/489/**

Thompson, P.R., 1980. Foraminifers from Deep Sea Drilling Project Sites 434, 435, and 436, Japan Trench. *In* von Huene, R., and Nasu, N., et al., *Init. Repts. DSDP,* 56, 57: Washington, DC (U.S. Govt. Printing Office), 775–807. **doi:10.2973/dsdp.proc.5657.122.1980**

Weinbauer, M.G., Beckmann, C., and Höfle, M.G., 1998. Utility of green fluorescent nucleic acid dyes and aluminium oxide membrane filters for rapid epifluorescence enumeration of soil and sediment bacteria. *Appl. Environ. Microbiol.*, 64(12):5000–5003. **http://aem.asm.org/cgi/content/abstract/64/12/5000/**

Winter, A., and Siesser, W.G., 1994. Atlas of living coccolithophores. *In* Winter, A., and Siesser, W.G. (Eds.), *Coccolithophores:* Cambridge (Cambridge Univ. Press), 107–159.

Publication: 4 October 2011
MS 331-102

Figure F1. Sample identification scheme, Expedition 331.

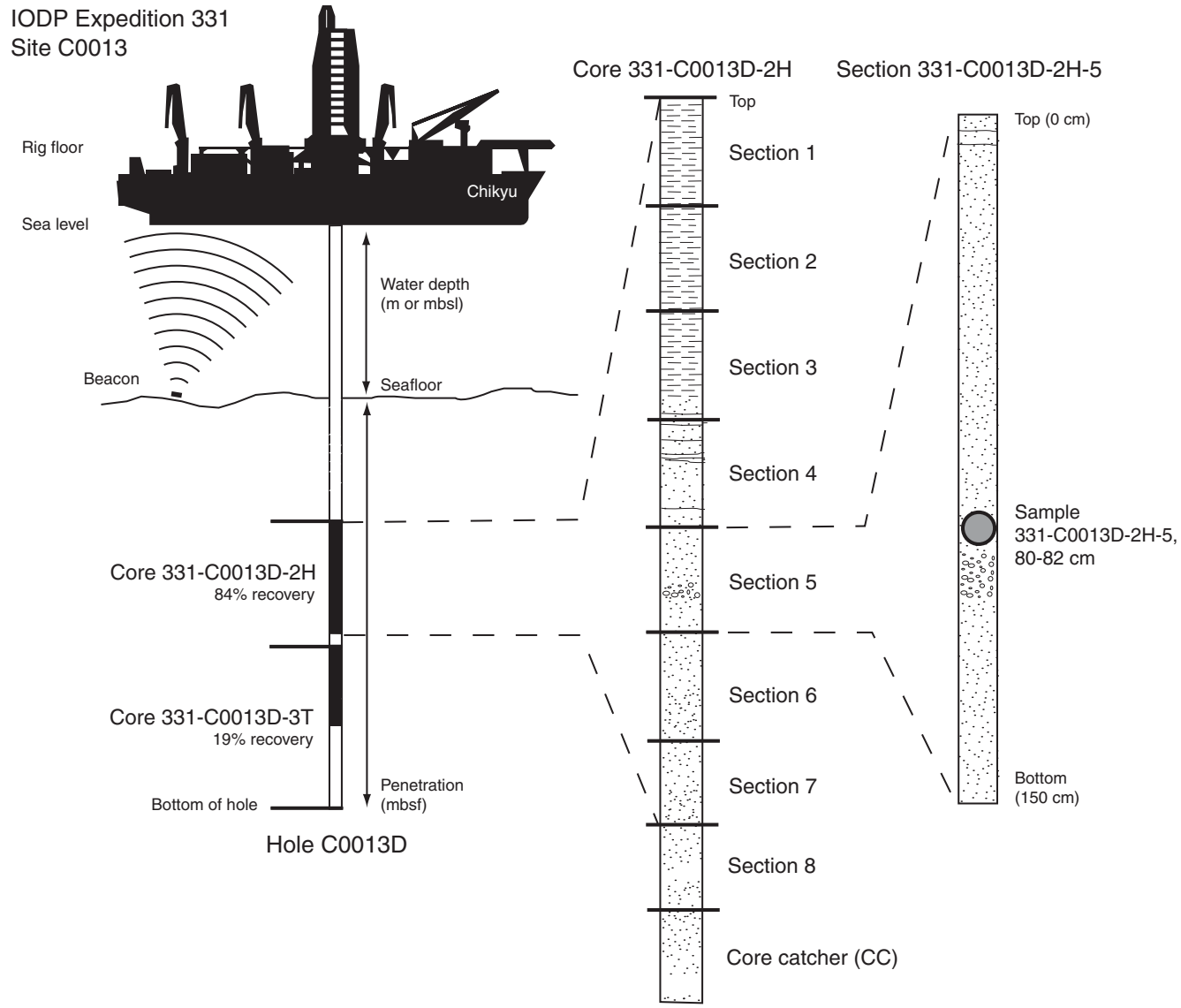

Figure F2. Core flow diagram, Expedition 331. X-CT = X-ray computed tomography, WRs = whole rounds, IW = interstitial water, MSCL-W = multisensor core logger for whole-round samples, MSCL-I = multisensor core logger imaging system, MSCL-C = multisensor core logger color spectrophotometer, VCD = visual core description, Alk = alkalinity, MAD = moisture and density, PWV = *P*-wave velocity, ICP = inductively coupled plasma spectroscopy, GC = gas chromatography, UV-Vis = UV visible, GC-FID = GC-flame ionization detector.

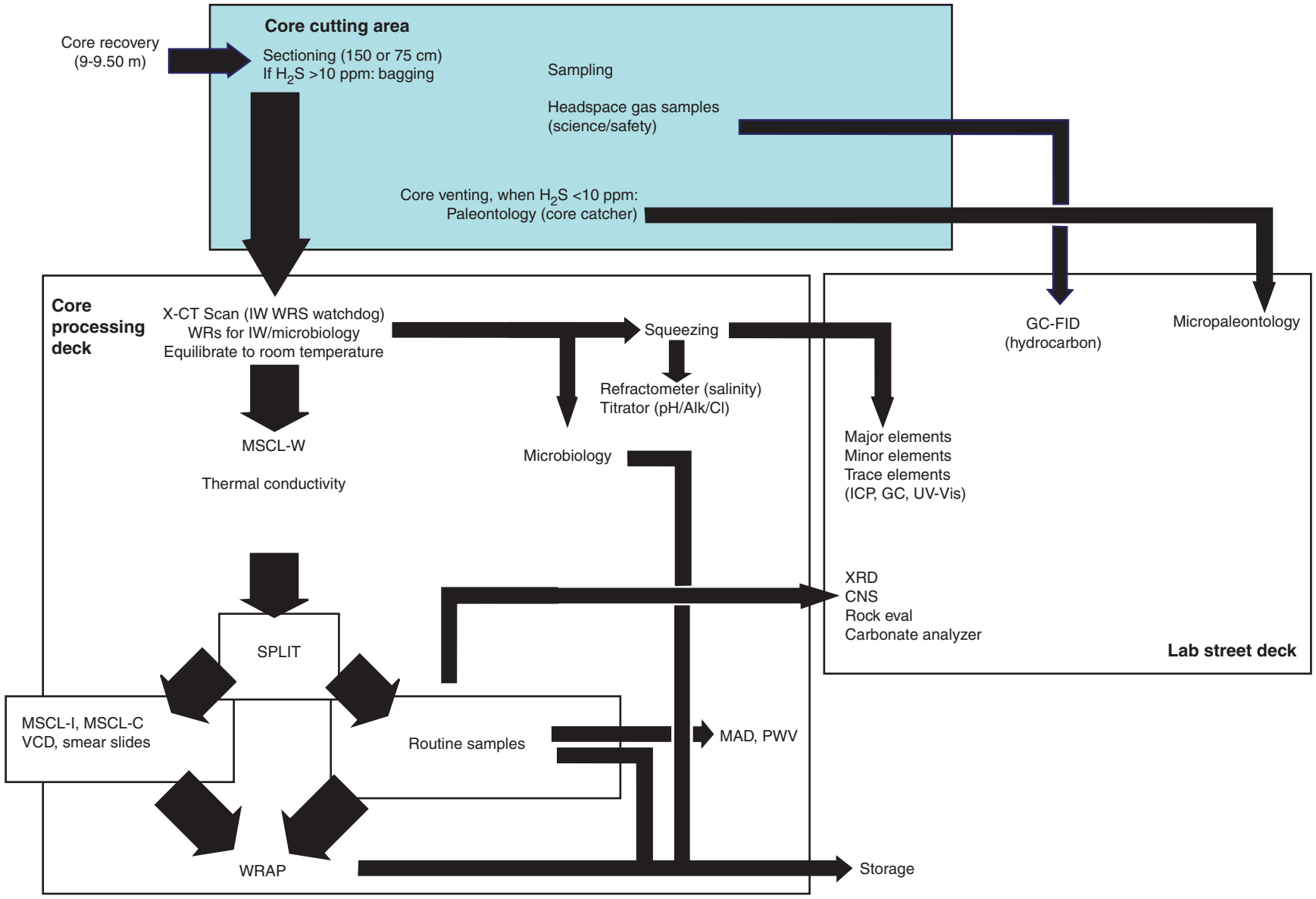

Figure F3. Graphic patterns and symbols used on visual core descriptions, Expedition 331. **A.** Graphic patterns. (Continued on next page.)

Lithology

Figure F3 (continued). B. Symbols.

Sedimentary structures

- Lithoclast
- Planar bedding (lamination)
- Chaotic bedding
- Fluid escape structure
- Inclined strata

Lithologic accessories/ Veins

- Vein
- Color banding
- Mud clasts
- Isolated mud clasts
- Pumice
- Pumice scattering
- Sand scattering
- Mottled/Motting
- Black band
- Calcareous
- Gl Glauconite

Drilling disturbance

- Slightly disturbed
- Moderately disturbed
- Heavily disturbed
- Slightly fractured
- Moderately fractured
- Highly fractured
- Drilling breccia
- Soupy
- Gas expansion
- Extruded
- Biscuit
- Flow-in
- X Drilling-induced void
- Melted plastic core liner

Shipboard samples

CARB	Inorganic carbon
HS	Headspace gas
IMP	Resistivity
IW	Interstitial water
PAL	Paleontology
MBIO	Microbiology
PP	Moisture and density
PWVD	P-wave velocity
SEM	Images for paleontology
SS	Smear slide
TS	Thin section
XRD	X-ray diffraction
XRF	X-ray fluorescence

Figure F4. Symbols used for alteration, sulfide, and sulfate logging, Expedition 331.

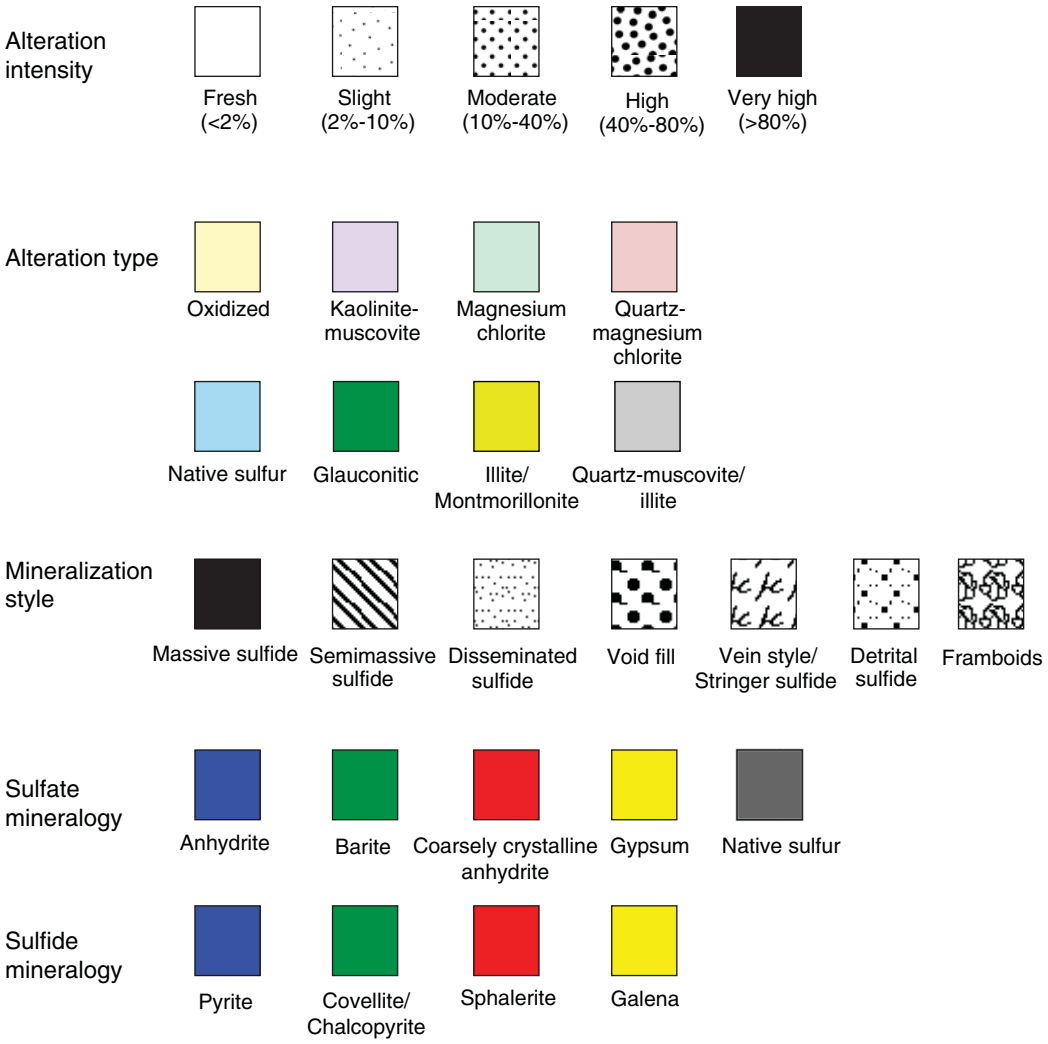

Table T1. Comparison of millimeter, phi, and Wentworth classification of grain size.

Grain size (mm)	Phi (ϕ)	Wentworth grain size classification (ϕ)
(1 km)	–20	
4096	–12	
1024	–10	Boulder (–8 to –12)
256	–8	Cobble (–5 to –8)
64	–6	
16	–4	Pebble (–2 to –5)
4	–2	
3.36	–1.75	
2.83	–1.5	Granule (–1 to –2)
2.38	–1.25	
2		
1.68	–0.75	
1.41	–0.5	Very coarse sand (0 to –1)
1.19	–0.25	
1	0	
0.84	0.25	
0.71	0. 5	Coarse sand (1 to 0)
0.59	0.75	
0.5	1	
0.42	1.25	
0.35	1.5	Medium sand (2 to 1)
0.3	1.75	
0.25	2	
0.21	2.25	
0.177	2.5	Fine sand (3 to 2)
0.149	2.75	
0.125	3	
0.105	3.25	
0.088	3.5	Very fine sand (4 to 3)
0.074	3.75	
0.0625	4	
0.053	4.25	
0.044	4.5	Coarse silt (5 to 4)
0.037	4.75	
0.031	5	
0.0156	6	Medium silt (6 to 5)
0.0078	7	Fine silt (7 to 6)
0.0039	8	Very fine silt (8 to 7)
0.002	9	
0.00098	10	Clay
0.00049	11	(Some use 2 µm or 9 as the clay boundary)
0.00024	12	
0.00012	13	

Table T2. Diagnostic features of alteration styles defined during Expedition 331.

Style of alteration	Diagnostic features
Oxidation	Affects near-surface rocks, resulting in a brownish to yellow coloration of fine sediments and localized orange to dark brown iron staining of larger clasts.
Glauconitic	Greenish staining of near-surface sediments. Note that the presence of glauconite was not confirmed by XRD.
Native sulfur	Significant yellow native sulfur present.
Kaolinite-muscovite	Hydrothermal alteration, resulting in pale gray clay. Kaolinite and/or muscovite identified by XRD.
Illite/Montmorillonite	Hydrothermal alteration, resulting in pale gray clay. Illite and/or montmorillonite identified by XRD.
Mg chlorite	Hydrothermal alteration, resulting in pale gray clay, which may have a distinct greenish or bluish tinge. Mg chlorite identified by XRD.
Quartz–Mg chlorite	Hard crystalline rocks with quartz veining and greenish clay alteration. Quartz and Mg chlorite identified by XRD.
Quartz-muscovite/illite	Hard crystalline rocks with intense silicification and a gray color. Quartz and muscovite/illite identified by XRD. Only seen at Site C0016.

XRD = X-ray diffraction.

Table T3. Styles of sulfide mineralization.

Style of alteration	Diagnostic features
Massive sulfide	Rocks containing >75% sulfide minerals.
Semimassive sulfide	Rocks containing >25%–75% sulfide minerals, which form aggregates or intergrowths.
Disseminated sulfide	Rocks containing 5%–25% disseminated sulfides.
Void fill	Minerals partially or totally filling a void (vesicle, etc.).
Vein/Stringer sulfide	Rocks containing sulfide in fractures.
Detrital sulfide	Clastic sulfide fragments in sediment.

Table T4. Chemical formulae of sulfide minerals identified during Expedition 331.

Mineral	Composition
Pyrite	FeS_2
Pyrrhotite	$Fe_{1-x}S$
Chalcopyrite	$CuFeS_2$
Covellite	CuS
Sphalerite	(Zn,Fe)S
Wurtzite	ZnS
Galena	PbS
Tennantite	$(Cu,Fe,Zn.Ag)_{12}As_4S_{13}$
Tetrahedrite	$(Cu,Fe,Zn.Ag)_{12}Sb_4S_{13}$
Sulfosalt	A class of sulfide minerals in which a semimetal (As or Sb) takes the place of one or more S atoms in the structure. Tennantite and tetrahedrite are important examples, and Pb and Ag commonly form sulfosalts.

Table T5. Analytical conditions for major element analysis of glass beads, Expedition 331.

Element line	Filter	Crystal	Peak angle (°)	Count time (s)	BG 1 (°)	Count time (s)	BG 2 (°)	Count time (s)	Detector
Si-Kα	Out	PET	108.946	40	106.100	10	111.250	10	PC
Ti-Kα	Out	LiF1	86.155	20	85.240	10	87.120	10	SC
Al-Kα	Out	PET	144.607	40	147.150	10	140.400	10	PC
Fe-Kα	Out	LiF1	57.535	20	58.180	10	56.900	10	SC
Mn-Kα	Out	LiF1	62.997	20	62.200	10	63.820	10	SC
Ca-Kα	Out	PET	45.154	40	43.650	10			PC
Mg-Kα	Out	RX25	38.804	40	40.750	10	36.900	10	PC
Na-Kα	Out	RX25	47.125	40	49.000	10	45.250	10	PC
K-Kα	A 140	PET	50.632	40	49.200	10			PC
P-Kα	Out	PET	89.280	40	91.350	10	87.200	10	PC

Analyses performed on the Supermini (Rigaku) X-ray fluorescence spectrometer. BG = background angle. PC = flow-proportioned counter, SC = scintillation counter.

Table T6. Average measured values and 3σ for major elements, Expedition 331.

Component	Reference value (100% normalized)	Measured value (average)	Standard deviation (3σ)	Relative standard deviation (%)
SiO_2	50.767	50.722	0.115	0.1
TiO_2	1.435	1.433	0.038	0.9
Al_2O_3	17.135	17.067	0.144	0.3
Fe_2O_3	11.775	11.770	0.075	0.2
MnO	0.176	0.181	0.006	1.1
CaO	9.753	9.791	0.044	0.2
MgO	5.170	5.076	0.151	1.0
Na_2O	2.720	2.747	0.177	2.1
K_2O	0.777	0.752	0.019	0.8
P_2O_5	0.293	0.279	0.014	1.7

Measured values determined on the Supermini (Rigaku) X-ray fluorescence spectrometer from 10 analyses of JB-3 standard.

Table T7. Detection limits of the direct cell counting for 100 fields under three representative conditions, Expedition 331.

Condition	T_{fov}/C_{fov}	ln(1 – p)	Final dilution rate	*n** (cells/mL sediment)
1	14,526	–2,996	1,500	6.53×10^5
2	14,526	–2,996	2,000	8.70×10^5
3	14,526	–2,996	3,000	1.31×10^6

* = lower detection limit.

Table T8. Concentrations of perfluorocarbon tracer (PFT) in drilling mud components used in Expedition 331.

Sample ID	Description	PFT in test vial gas phase (ppm)	Sample weight in test vial (g)	PFT per g sample (ppm)
C0013B-1LMW	1.30s.g SWG (with PFT)	5.23E+02	6.3115	8.29E+01
C0013B-2LMW	1.30s.g SWG (with PFT)	4.20E+02	6.6896	6.28E+01
C0013B-5LMW	1.03s.g GuarGuam (with PFT)	8.03E+00	4.6341	1.73E+00
C0013B-6LMW	1.03s.g GuarGuam (with PFT)	6.97E+00	5.2016	1.34E+00
C0013D-1LMW	GuarGuam (rester) (with PFT)	1.27E+02	3.6449	3.48E+01
C0013D-3LMW	1.04s.g SWG	8.01E+01	1.6684	4.80E+01
C0013D-4LMW	1.04s.g SWG	1.18E+02	2.7956	4.22E+01
C0013E-1LMW	1.03s.g GuarGuam	3.67E+02	5.4688	6.71E+01
C0013E-2LMW	GuarGuam (rester) (with PFT)	2.85E+02	3.2465	8.79E+01
C0013E-3LMW	GuarGuam (rester) (with PFT)	6.36E+02	5.2393	1.21E+02
C0013E-4LMW	GuarGuam (rester) (with PFT)	1.48E+01	5.6186	2.63E+00
C0013E-5LMW	SeawaterGel (unweighted) (with PFT)	4.01E+00	5.1367	7.81E–01
C0013E-6LMW	GuarGuam (rester) (with PFT)	7.80E+01	5.6737	1.37E+01
C0014B-1LMW	SeawaterGel (unweighted) (with PFT)	2.34E+02	4.3789	5.34E+01
C0016B-1LMW	GuarGuam with PFT	9.42E+00	6.5877	1.43E+00
C0016B-2LMW	GuarGuam mud with PFT	1.93E–01	2.059	9.37E–02

MW = mud water. SWG = seawater gel.